Published in final edited form as:
J Phys Chem C Nanomater Interfaces. 2009 ; 113(41): 17761–17767. doi:10.1021/jp905776g.

Effects of shape and size of cobalt ferrite nanostructures on their MRI contrast and thermal activation

Hrushikesh M. Joshi[a,§], **Yen Po Lin**[a,§], **Mohammed Aslam**[b], **P. V. Prasad**[c], **Elise A. Schultz-Sikma**[d], **Robert Edelman**[c], **Thomas Meade**[d], and **Vinayak P. Dravid**[a,e,*]

[a] Dept. of Materials Science & Engineering, Northwestern University, Evanston, IL 60208, USA

[b] Dept. of Physics, Indian Institute of Technology Bombay, Powai, Mumbai-400076, INDIA

[c] Department of Radiology, Evanston Northshore Healthcare, Evanston, IL 60201, USA

[d] Dept. of Chemistry, Northwestern University, Evanston, IL 60208, USA

[e] International Institute for Nanotechnology, Northwestern University, Evanston, IL 60208, USA

Abstract

Cobalt ferrite magnetic nanostructures were synthesized via a high temperature solution phase method. Spherical nanostructures of various sizes were synthesized with the help of seed mediated growth of the nanostructures in organic phase, while faceted irregular (FI) cobalt ferrite nanostructures were synthesized via the same method but in the presence of a magnetic field. Magnetic properties were characterized by SQUID magnetometry, relaxivity measurements and thermal activation under RF field, as a function of size and shape. The results show that the saturation magnetization of the nanostructures increases with an increase in size, and the FI nanostructures exhibit lower saturation magnetization than their spherical counterparts. The relaxivity coefficient of cobalt ferrite nanostructures increases with increase in size; while FI nanostructures show a higher relaxivity coefficient than spherical nanostructures with respect to their saturation magnetization. In the case of RF thermal activation, the specific absorption rate (SAR) of nanostructures increases with increase in the size. The contribution sheds light on the role of size and shape on important magnetic properties of the nanostructures in relation to their biomedical applications.

Keywords

Cobalt ferrite; shape; size; thermal activation; MRI contrast agent

Introduction

Functional nanostructures have attracted considerable attention in the recent decade; not only because of fundamental scientific interest in relation to size/shape effects, but also for their potential technological applications in many important fields[1–3]. In particular, due to their unusual magnetic properties and ability to respond at the molecular level, magnetic nanostructures are potential candidates for biomedicine such as targeted drug delivery[4], diagnostics[5], and magnetic separation.[6] They are also being explored as contrast agents in MRI[7], thermo responsive drug carriers[8] as well as in the thermal activation therapy of cancer.[9] Such applications are enabled due to truly nanoscale properties of magnetic

* Author to whom correspondence should be addressed, v-dravid@northwestern.edu Tel: +1-847-467-1363 Fax: 1-847-467-6573.
§ Authors contributed equally.

materials, principally their superparamagnetic behavior at nanometer scale. However the role of shape anisotropy has not been extensively explored or exploited for superparamagnetic nanostructures. The focus of this contribution is the designed synthesis protocol that can control the growth of these nanostructures for desired properties.

Many advances to synthesize magnetic nanostructures have been made using variety of chemical approaches, including co-precipitation method[10], Sol-gel process[11], hydrothermal synthesis[12], high temperature reactions[13], microwave irradiation synthesis [14], and polyol methods[15], among others. These methods manipulate various experimental parameters such pH of the solution, ionic strength, capping agent, reaction temperature and pressure to control the size and shape evolution of nanostructures.

Recently, Sun *et al* [16] have developed a high temperature solution phase method that can precisely synthesize monodisperse nanostructures of diverse materials; which has led of to flurry of reports on chemical synthesis of various sizes and shapes.[17, 18] It has been shown that seed mediated growth is an effective method for the synthesis of size controlled monodispersed nanoparticles. Magnetic properties of the magnetic nanostructures are dependent on their shape because of the role of crystallographic and shape anisotropy in magnetism. Zeng *et al* [19] controlled shape of $MnFe_2O_4$ nanostructures by controlling the surfactant to precursor ratio, Similar effort were done by Song *el al* [20] in which the synthesis of spherical and cubic cobalt ferrite nanostructures were performed using seed mediated growth approach. In their work, shape of the nanostructures was interchanged between spherical and cubic shapes by controlling the nanostructures growth rate.[20] Choi *et al* [21] demonstrated modulation of magnetism by controlling the aspect ratio of the magnetic nanostructures. In another report, Cheon *et al* [22] demonstrated a size and shape dependent synthesis of cobalt nanostructures by adjusting kinetic and thermodynamic parameters such as growth temperature, time and capping molecules. This report suggests magnetic properties such as coercive field H_c, superparamagnetism, ferromagnetism depend on the size and shape of nanoparticles. In the case of magnetic nanostructures, application of external magnetic field is an additional growth controlling factor that can engineer the size and shape of the particle. Wang *et al* [23] have reported ferromagnetic Fe_3O_4 nanowires by hydrothermal process with the application of an external magnetic field.

An important field of potential application of magnetic nanostructures is MRI contrast enhancement. Magnetic resonance imaging is a powerful non-invasive imaging technique which is used as a diagnostic and imaging tool in medical research. It is based on the response of proton spin in the presence of an external magnetic field when triggered with a radio frequency pulse. Under the external magnetic field influence, protons align in one direction. Upon the application of the RF pulse, aligned protons perturb and returns back to their original state. This phenomenon is called the relaxation process. There are two independent relaxations processes i.e. longitudinal and transverse relaxation processes, which is used to generate MR image. Any local magnetic field variation leads to local variation in relaxation, results into corresponding image contrast. A large magnetic susceptibility difference between the nanostructures and their surrounding medium leads to a microscopic magnetic field gradient. Protons that diffuse from these field gradients result in dephasing of the proton magnetic moments that lead to a negative contrasting effect (darkening of image) in MRI.[4] Nanostructures that cause this are known as T_2 contrast agent. Magnetic nanostructures have the ability to affect the relaxation process and thus can be used as contrast agent upon accumulation in tissue. Recently, Wan *et al* [24] demonstrated magnetite r_2 relaxivity of about ~ 82 $mM^{-1}s^{-1}$. Some of us reported that the r_2 values of their iron oxide nanostructures synthesized by amine-stabilized aqueous method were 80~232 $mM^{-1}s^{-1}$.[25] Cheon *et al*[26] reported the size dependent magnetic properties as well as MR properties of water soluble iron oxide nanostructures. The same group synthesized

$MnFe_2O_4$, $FeFe_2O_4$, $CoFe_2O_4$, and $NiFe_2O_4$ nanostructures and found that contrast enhancement is generally greatest for manganese ferrite nanostructures.[7]

Another specific application has drawn considerable interest due to its noninvasive methodology in the thermal activation of cancerous cells at 5 – 7 °C above the body temperature.[9] With the help of magnetic nanostructures, less side effects, selective targeting and localized heating of cancerous cells can be achieved. In particular spinel ferrite particles have attracted considerable interest due to their nontoxicity, biocompatibility and thermal activation figure of merit (SAR) in the presence of an radiofrequency (RF) magnetic field.[9,27] Surprisingly, Lee *et. al.* [28] demonstrated self heating of cobalt ferrite nanostructures of 165 nm size cobalt ferrite nanostructures. Veverka *et al* [29] correlated the SAR of cobalt ferrite nanostructures with temperature dependent AC losses. In another effort, Skumiel [30] showed the H^2 law type dependence of SAR on the square amplitude of the magnetic field to the presence of superparamagnetic cobalt ferrite nanostructures in the fluid. Fortine *et al* [31] have performed detailed calculations as well as experimental demonstration of effect of medium, viscosity and size of the nanostructure on SAR of magnetic nanostructures specially cobalt ferrite nanostructures. More recently Kim *et al*[32] have reported dependence of thermal activation of cobalt ferrite nanoparticles on magnitude and frequency of applied magnetic field. However, very little has been explored on the effect of shape on SAR of cobalt ferrite nanostructures.

Considering the versatile applications of magnetic nanostructures in diagnostics and therapeutics, it is very important to tailor the magnetic properties of the nanostructures for their use as multifunctional probes for biomedicine. In this contribution, we report synthesis of cobalt ferrite nanostructures by the high temperature solution phase method. Spherical nanostructures of various sizes were synthesized with the help of seed mediated growth of the nanostructures in organic phase, while FI cobalt ferrite nanostructures were synthesized with the same method but in the presence of a magnetic field. The saturation magnetizations of cobalt ferrite nanostructures were characterized by SQUID. MRI relaxivity measurements as well as the thermal-activation of ferrite nanostructures with the help of RF generator were investigated with different sizes and shapes of the nanostructures for their essential attributes, for applications in biomedicine.

Experimental Methods and Materials

a. Nanoparticle synthesis and surface functionalization

Iron(III) acetylacetonate, cobalt(III) acetylacetonate, dodecylamine, lauric acid, 1,2-hexadecanediol, Benzyl ether were obtained from Aldrich Chemicals and used without modifications.

Nanostructures of different sizes were synthesized by seeded-growth thermal decomposition [16]. Iron(III) acetylacetonate (4mmol) and cobalt(III) acetylacetonate (2 mmol) were used as a precursor to make $CoFe_2O_4$ nanostructures. Three surfactants, dodecylamine (12mmol), lauric acid (12mmol), and 1,2-hexadecanediol (20mmol) were added to stabilize nucleation and growth. Benzyl ether (40ml) was used as the solvent. The solution was heated to 230 °C for 2 hours with a flow of nitrogen gas to prevent oxidation, and then raised to 280 °C for 1 hour. The molar ratio of cobalt (III) acetylacetonate and iron (III) acetyalacetonate is 1:2. The resulting nanostructure diameters were 5 to 7 nm. The magnetic nanostructures were precipitated out from the solvent through external magnetic field. To grow larger particles, 60mg of the nanostructure seed was mixed with Iron (III) acetylacetonate (0.57 mmol), dodecylamine (1.71 mmol), lauric acid (1.71 mmol), and 1,2-hexadecanediol (2.86 mmol) in benzyl ether (40 ml). In the growth reaction, the solution was heated directly to 280 °C for 3

hr without holding at 230 C. Nanostructure size could be further increased by repeating the growth reaction.

The particles made by the above method are spherical. Shape change was achieved by adding a magnetic stirrer bar during the synthesis.

Phase transfer of magnetic nanostructures was done using 11-amino undecanoic acid. Small amount of 11-aminoundecanoic acid was dissolved in 1 ml of ethyl alcohol. Equal amount of magnetic nanostructures were redispersed in 1 ml of hexane. Resulting biphasic mixture was subjected to vigorous shaking for 24 hours. Magnetic nanostructures were separated out with the help of strong magnet and again redispersed in water. The resulting aqueous nanostructures solution is stable for several months.

b. Materials characterization

A Hitachi HF-2000 Transmission Electron Microscope (TEM) was used to characterize the nanostructures using image mode. The nanostructure diameters were determined by the statistical averaging using Digital Micrograph. In the case of FI nanostructures longest diagonals were recorded.

A Superconducting Quantum Interference Device (SQUID) magnetometer was used to obtain the hysteresis of the samples at room temperature. The applied external field ranged from −2 Tesla to 2 Tesla.

Nanostructures were dispersed in water and then diluted to concentrations ranging from 0.01 to 0.3 mM of metal ion. A GE Sigma 3.0 HDxt MR System was used to scan the nanostructure solutions using multiple-echo-fast-spin-echo sequence to determine T_2 values.

Thermal activation and SAR measurements

Thermal activation experiments were performed on various shapes and sizes of cobalt ferrite nanostructures to determine the specific absorption rate. All AC magnetic field thermal experiments were performed on an MSI automation Inc., Hyperthermia Research System (model hyper 5) RF generator at a frequency of 300 KHz and 5 kW of power. 3 ml of suspension was taken in a double walled glass jacket where space between both the walls was evacuated to minimize the heat loss. This jacket was then placed inside the coil generating AC magnetic field. A nonmagnetic nonmetallic optical temperature probe (Fiso) was used to monitor the temperature. Each experiment time duration was 60 minutes. Heat generated during the thermal activation is measured in terms of Specific Absorption Rate (SAR).

Specific absorption rate is the heating ability of magnetic materials in the presence of an AC magnetic field and is defined as the amount heat generated per unit gram of magnetic material per unit time [9a, 28], i.e.

$$SAR = \frac{CV_s}{m}\left(\frac{dT}{dt}\right) \quad (1)$$

Where C is the sample specific heat capacity, in this case water having value 4.18 $Jg^{-1}\,C^{-1}$, dT/dt is initial slope of temperature verses time graph, V_s is the sample volume and m is mass of magnetic material in the sample.

Results and discussion

As the first step, spherical nanostructures of 6 nm size were synthesized to serve as seeds for further growth of the nanostructures. Nanostructures of various shapes and sizes were characterized by transmission electron microscopy.

Figure 1a, b and c represents spherical nanostructures (grown without external magnetic field) of size 6 ±1.0 nm, 10 ±1.5 nm and 15 ±2.0 nm while figure 1d, e shows FI nanostructures (grown in the presence of external magnetic field) of size 12±2.0 nm, 25±2.0 nm respectively. From the TEM micrographs, it is apparent that (figure 1d-e) nanostructures grown in the presence external magnetic field show faceted and sharp corners compared to spherical nanostructures. Wang *et al*[23] observed similar results when they applied strong magnetic fields (0.15 ~ 0.35 T) during synthesis, which resulted in Fe_3O_4 nanowires. Since weak external magnetic field was used during synthesis, the aspect ratio of resulting FI nanostructures is not high. This may be due to the Lorentzian forces influencing individual ions in organic phase leading to preferential growth of cobalt ferrite nanostructures in the presence of external magnetic field.[23] The preferential growth of crystal towards certain planes results into breaking of shape isotropy.

The Field dependent magnetization measurements were performed to quantify saturation magnetization (Ms) of various shape and sizes of cobalt ferrite nanostructures. The Ms values are summarized in table 1. Table 1 and figure 2 show that saturation magnetization increases with particles size. It is also interesting to note that FI nanostructures possess lower M_s values than spherical nanostructures but the magnetization is clearly rising with field at this field value (20 000 Oe), as against in the case of spherical nanoparticles it is almost saturated. One possible reason for lower magnetization is, in magnetic field-assisted synthesis, preferential growth of towards easy magnetized crystallographic direction induces the higher shape anisotropy, favoring magnetization along easy axis of magnetization than other crystallographic directions.

Partial pinning of magnetic moments and difficulty in aligning in external magnetic field might be other possible reasons for reduced magnetization of these structures. Another important observation is that all FI cobalt ferrite nanostructures have non-zero remanence as indicated by presence of hysteresis in hysterisis loop.

The stable cobalt ferrite nanostructures of various shapes and sizes were phase transferred from organic phase to aqueous phase using method described previously. Phase transferring as well as capping agent i.e. amino undecanoic acid agent kept nanostructures stable suspension in aqueous phase. Aqueous phase solution of cobalt ferrite nanostructures were used for MRI and thermal activation experiments.

The contrast enhancing efficacy of the synthesized spherical and FI cobalt ferrite nanostructures (T_2 agent) is characterized by its relaxivity coefficient (r_2), which is related to T_2 through the equation, [24]

$$\frac{1}{T_2}=\frac{1}{T_2^0}+r_2C \tag{2}$$

Where, C is the contrast agent concentration, T_2 is observed relaxation time in the presence of cobalt ferrite nanostructures while T_2^0 is relaxation rate of pure water. In Equation 2, T_2 becomes shorter when concentration (C) increases, while r_2 is relaxivity coefficient. From the given equation it reveals that as the concentration increases MRI image appears darker

and contrast agents having higher r_2 value require small concentration increments. In other words, unlike T_2, which depends on concentration, r_2 is a concentration-independent term. A contrast agent with a large r_2 can shorten T_2 drastically with a smaller concentration increment.

Figure 3 shows the plot of $1/T_2$ Vs metal ion concentration (Co + Fe). Relaxivity coefficients of r_2 were determined by the slops of straight line connecting the different point in the plot. Relaxivity of the chemically synthesized cobalt ferrite nanostructures were compared with commercially available contrast agent, ferumoxytol. Figure 3 shows that $1/T_2$ and concentration has a linear relationship. Figure 3 shows r_2 values which range from 110 – 345 $mM^{-1}s^{-1}$ for the cobalt ferrite nanostructures. r_2 values of cobalt ferrite nanostructures are higher than ferumoxytol (91 $mM^{-1}s^{-1}$). It also reveals that relaxivity coefficient increases with increase in nanostructure size.

To compare the r_2 values of different sizes and shapes of the nanostructures r_2 values were plotted against size of the nanostructures (figure 4). As shown in figure 4, r_2 increases with particles size i.e. from 110 – 301 $mM^{-1}s^{-1}$ for spherical nanostructures while 155 – 345 $mM^{-1}s^{-1}$ for FI nanostructures, which are consistent with previously reported results.[26]

Many researchers related increasing r_2 values to greater nanostructure saturation magnetization values (M_s).[33] Nanostructures with greater magnetic moments strongly disturb the in-phase precession of the neighboring nuclei, resulting in faster T_2 relaxation. To examine above relation, values of r_2 were plotted against values of magnetic saturation of respective magnetic nanostructures.

Figure 5 shows r_2 increases with increase in Ms value. Interestingly another important observation is that magnitudes of r_2 values of FI nanostructures are greater than spherical nanostructures while their Ms values are lower than spherical nanostructures. This suggests that relaxivity coefficient is not only dependent on magnetic saturation of the nanostructures but also affected by its geometry.

Faster relaxation of protons may be because of the magnetometer measurements failed to reflect this due to partial pinning as discussed previously. FI nanostructures have faceted morphology with large amount of sharp edges and corners which may be creating the pseudo magnetic charges on the surface in similar manner as that of cube shape nanostructures[34] and that may results into higher gradient of magnetic field in these regions leading to higher relaxation of protons. Another possible explanation is that FI nanostructures have greater surface-to-volume ratio and greater number of hydrogen nuclei of water in proximity. Therefore, a greater number of neighboring nuclei were disturbed by the nanostructures magnetic field, resulting in faster relaxation.

Various cobalt ferrite nanostructures were subjected to alternating current magnetic field for thermal activation. In thermal activation of cobalt ferrite nanostructures, increase in temperature is collective effect of different loss processes (hysteresis losses, Néel and Brownian relaxation). In the present case, hysterisis losses can be neglected due to their negligible contributions.

In the case of magnetic nanostructures, Brownian and Néel relaxation processes are responsible for thermal activation process. In Brownian relaxation process, thermal response is generated due to mechanical friction with surrounding medium when nanostructures keep oscillating towards the field keeping the its magnetic moment fix along the crystal axis. The Brownian relaxation time τ_B is given by: [28]

$$\tau_B = \frac{3\eta V_H}{kT} \tag{3}$$

Where η is the viscosity, V_H is the hydrodynamic volume of the particles, *k* is boltzman constant, T is temperature. While, Néel relaxation is thermal response, which is generated due to the internal fluctuations of the magnetic moment with respect to the crystal lattice.[35]

The Néel relaxation time is given by τ_N

$$\tau_N = \tau_0 e^{\frac{KV}{kT}} \tag{4}$$

Where, $\tau_0 \approx 10^{-9}$ s, K is the anisotropy constant of magnetic materials, V is the volume of the magnetic particle.

However, effective relaxation time τ is calculated by,

$$\frac{1}{\tau} = \frac{1}{\tau_N} + \frac{1}{\tau_B} \tag{5}$$

Therefore, thermal activation is dominated by shorter relaxation time. According to theoretical calculations and previously observed facts, in the case of cobalt ferrite nanostructures, effective relaxation τ is governed by Néel relaxation below 7–9 nm size while above this size regime, Brownian relaxation is the dominating factor.[31] Since all the nanostructures synthesized in the given studies are equal or above 7–9 nm size, Brownian relaxation is dominating factor for thermal activation of cobalt ferrite nanostructures.

Heat generated during the thermal activation of nanostructures was determined by SAR as given in the equation 1.

For monodisperse nanoparticles, analytical relationship between SAR and different parameters is given by[31]

$$SAR = \frac{P}{\rho\varphi} = \frac{\mu_0 \chi_0 H_0^2}{2\rho\varphi} \omega \frac{\omega\tau}{1+(\omega\tau)^2} \tag{6}$$

Where P mean volumetric power dissipation, ρ, the mass per unit volume of iron oxide, φ, the volume fraction of particles in the suspension,μ_0, the vacuum magnetic permeability,χ_0, static susceptibility, H_0 is the magnetic field, ω is the frequency and τ is the relaxation time.

Where, χ_0 was assumed to be chord susceptibility and is given by,

$$\chi_0 = \frac{(\mu_0 m_s^2 \phi V)}{kT} \frac{(\coth\xi - \frac{1}{\xi})}{\xi} \tag{7}$$

Where, V, volume, T, temperature & ξ is the langevin parameter. The replacement of chord susceptibility in equation 6 gives us the direct relation between m_s and the SAR.

When the particles are polydispersed, SAR can be adjusted by a log normal distribution of particle diameter 'd' and is given by,

$$y(d)=\frac{1}{\sqrt{2\pi}\sigma d}\exp\left[-\frac{\ln^2\left(\frac{d}{d_0}\right)}{2\sigma^2}\right] \quad (8)$$

y(d) represent the particles size distribution, σ, polydispersity index & d, is the particle diameter,

From the above equation, it can be easily seen that SAR is directly proportional to the magnetic saturation, inversely proportional to the polydispersity index and viscosity of the medium.

Figure 6 shows the plot of time versus change in temperature when cobalt ferrite nanostructures were placed in alternating current magnetic field. Observations such as size of nanostructures, saturation magnetization, and SAR are tabulated for comparison.

It is clear from figure 6 that initially temperature of all samples increased very rapidly while after some period of time it becomes saturated. Figure 6 and table 2 show that initially, the rate of temperature increase as well as SAR are higher for larger nanostructures than that of smaller nanostructures until 15 nm size particles while FI 25 nm size nanostructures show less SAR. However, it is also observed that FI structures are having lesser SAR values than spherical nanoparticles closer to its size.

The above observation suggests that thermal activation of cobalt ferrite nanostructures is strongly dependent on the shape of the particles as well as magnetic saturation values of the nanoparticles.[31] It is also interesting to note that SAR of FI 12 nm particles is lower than SAR of spherical 10 nm size cobalt ferrite nanostructures. According to the equation 6, 7 and 8, SAR is inversely proportional to the polydispersity index of the nanostructures since FI nanostructures have considerable irregular and faceted morphology, this might be leading to less SAR value.[31] Less saturation magnetization value of 12 nm FI nanostructures as compared to the 10 nm size spherical nanostructures is another possible reason for reduced SAR. Above observations suggest that, thermal activation not only depend on the size of the particles but also dependent on the overall contribution of size, geometry and magnetic properties of the nanostructures. However, quantitative shape dependent properties of magnetic nanostructures are under investigation.

Summary and Conclusions

Various shapes and sizes of cobalt ferrite nanostructures were synthesized by the high temperature solution phase method. Spherical nanostructures of various sizes were synthesized through seed mediated growth, while FI cobalt ferrite nanostructures were synthesized with same method but in the presence of a magnetic field. FI nanostructures behave differently than spherical nanostructures. FI nanostructures show less saturation magnetization than spherical nanostructures in ordinary conditions of magnetic measurements. In spite of lower saturation magnetization, FI nanostructure shows higher contrast effect and relaxivity coefficient than spherical nanostructures when compared with respect to their saturation magnetization values. SAR of nanostructures increases with

increase in the size of particles until certain size limit of the particles and decreases beyond that limit. Thus thermal activation of the cobalt ferrite nanostructures is strong function size, shape and magnetic properties of the nanostructures.

Acknowledgments

This research is supported by NSF-MWN (Grant No. DMR-0603184) and by the Center for Cancer Nanotechnology Excellence (CCNE) initiative of the National Institutes of Health's National Cancer Institute under Award U54CA119341 at Northwestern University. Any opinions, findings, and conclusions or recommendations expressed in this material are those of the author(s) and do not necessarily reflect those of the National Institutes of Health. Part of this work was performed in the EPIC/NIFTI facility of the NU*ANCE* centre (supported by NSF-NSEC, NSFMRSEC, Keck Foundation, the State of Illinois, and Northwestern University) at Northwestern University. MA would like to thank IIT Bombay and CSIR, India for financial support.

References

1. Hirsch LR, Stafford RJ, Bankson JA, Sershen SR, Rivera B, Price RE, Hazle JD, Halas NJ, West JL. Proc Nat Acad Sci. 2003; 100:13549–13554. [PubMed: 14597719]
2. Jain PK, Huang X, El-Sayed HI, El-Sayed MA. Acc Chem Res. 2008; 41:1578–1586. [PubMed: 18447366]
3. Bruchez M Jr, Moronne M, Gin P, Weiss S, Alivisatos AP. Science. 1998; 281:2013–2016. [PubMed: 9748157]
4. Sun C, Lee JSH, Zhang M. Adv Drug Deliv Rev. 2008; 60:1252–1265. [PubMed: 18558452]
5. Rosi NL, Mirkin CA. Chem Rev. 2005; 105:1547–1562. [PubMed: 15826019]
6. Molday RS, Mackenzie D. J Immun Meth. 1982; 52:353–367.
7. Lee AH, Huh YM, Jun YW, Seo JW, Jang JT, Song HT, Kim S, Cho EJ, Yoon HG, Suh JS, Cheon J. Nat Med. 2007; 13:95–99. [PubMed: 17187073]
8. Schmidt AM. Colloid Poly Sci. 2007; 285:953–966.
9. a) Prasad NK, Rathinasamy K, Panda D, Bahadur D. J Mater Chem. 2007; 17:5042–5051. b) Jordan A, Scholz R, Wust P, Fahling H, Krause J, Wlodarczyk W, Sander B, Vogl TH, Felix R. Int J Hyperthermia. 1997; 13:587–605. [PubMed: 9421741]
10. Sahoo Y, Goodarzi A, Swihart MT, Ohulchanskyy TY, Kaur N, Furlani EP, Prasad PN. J Phys Chem B. 2005; 109:3879–3885. [PubMed: 16851439]
11. Niederberger M. Acc Chem Res. 2007; 40:793–800. [PubMed: 17461544]
12. Daou TJ, Pourroy G, Bgin-Colin S, Grenche JM, Ulhaq-Bouillet C, Legar P, Bernhardt P, Leuvrey C, Rogez G. Chem Mater. 2006; 18:4399–4404.
13. Roca AG, Morales MP, Grady KO, Serna CJ. Nanotechnology. 2006; 17:2783–2788.
14. Khollam YB, Dhage SR, Potdar HS, Deshpande SB, Bakare PP, Kulkarni SD, Date SK. Mat Lett. 2002; 56:571.
15. Wei C, Wan J. J coll Inter Sci. 2007; 305:366.
16. Sun S, Zeng H, Robinson DB, Raoux S, Rice PM, Wang SX, Li G. J Am Chem Soc. 2004; 126:273–279. [PubMed: 14709092]
17. Bao N, Shen L, Wang Y, Padhan P, Gupta A. J Am Chem Soc. 2007; 129:12374–12375. [PubMed: 17880220]
18. Si S, Li C, Wang X, Yu D, Peng Q, Li Y. Cryst Growth Des. 2005; 5:391–393.
19. Zeng H, Rice PM, Wang SX, Sun S. J Am Chem Soc. 2004; 126:11458–11459. [PubMed: 15366890]
20. Song Q, Zhang ZJ. J Am Chem Soc. 2004; 126:6164–6168. [PubMed: 15137781]
21. Choi J, Oh SJ, Ju H, Cheon J. Nanolett. 2005; 5:2179–2183.
22. Park J, Kang NJ, Jun YW, Oh SJ, Ri HC, Cheon JC. hemphyschem. 2002; 3:543–547.
23. Wang J, Chen Q, Zeng C, Hou. Adv Mat. 2004; 16:137–140.
24. Wan J, Wei C, Mengb AX, Liu E. Chem Commun. 2007:5004–5006.
25. Aslam M, Schutz EA, Sun T, Meade T, Dravid VP. Cryst Growth Des. 2007; 7:471–475.

26. Jun YW, Huh YM, Choi JS, Lee JH, Song HT, Kim S, Yoon S, Kim KS, Shin JS, Suh JS, Cheon J. J Am Chem Soc. 2005; 127:5732–5733. [PubMed: 15839639]
27. Pradhan P, Giri J, Samanta G, Sarma HD, Mishra KP, Bellare J, Banerjee R, Bahadur D. J Biomed Mat Res Pt B: Appl Biomat. 2007; 81B:12–17.
28. Lee SW, Bae S, Takemura Y, Shim IB, Kim TM, Kim J, Lee HJ, Zurn S, Kim CS. J Mag Mag Mat. 2007; 310:2868–2870.
29. Veverka M, Veverka P, Kaman O, Lan cok A, Zaveta K, Pollert E, Knızek1 K, Bohacek J, Benes M, Kaspar P, Duguet E, Vasseur S. Nanotech. 2007; 18:345704–345711.
30. Skumiel A. J Mag Mag Mat. 2006; 307:85–90.
31. Fortin JP, Wilhelm C, Servais J, Ménager C, Bacri JC, Gazeau F. J Am Chem Soc. 2007; 129:2628–2635. [PubMed: 17266310]
32. Kim DH, Nikles DE, Johnson DT, Brazel CS. J Mag Mag Mat. 2008; 320:2390–2396.
33. Jun YW, Seo SW, Cheon J. Acc Chem Res. 2008; 41:179–189. [PubMed: 18281944]
34. Snoek E, Gatel C. Nano Lett. 2008; 8:4293–4298. [PubMed: 19367882]
35. Mornet S, Vasseur S, Grasset F, Duguet E. J Mater Chem. 2004; 14:2161–2175.

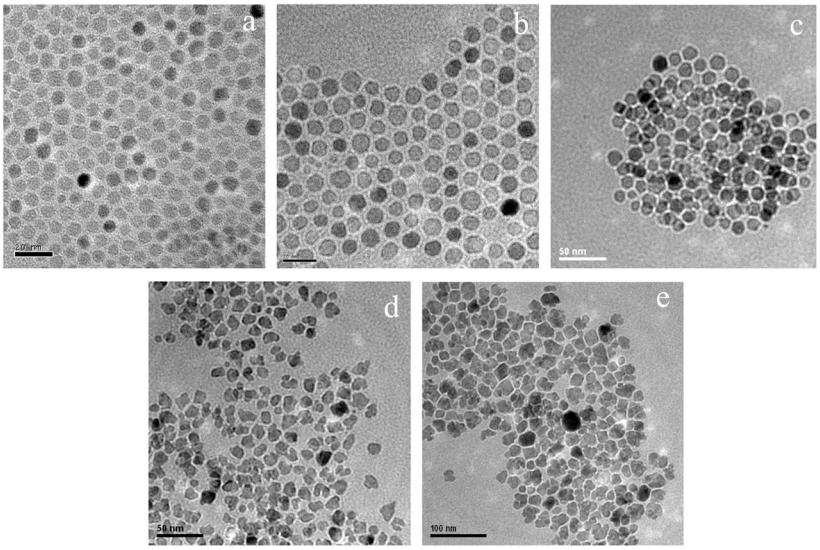

Figure 1.
$CoFe_2O_4$ nanostructures synthesized without (a-c) and with (d, e) magnetic field

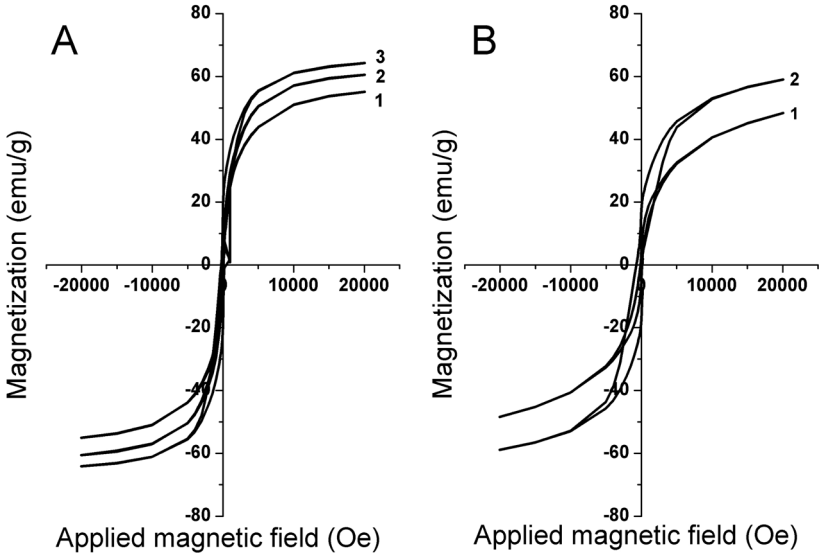

Figure 2.
Hysteresis curves of $CoFe_2O_4$ nanostructures. A: Spherical nanostructures 1) 6 nm 2) 10 nm 3) 15 nm B) FI nanostructures 1) 12 nm 2) 25 nm.

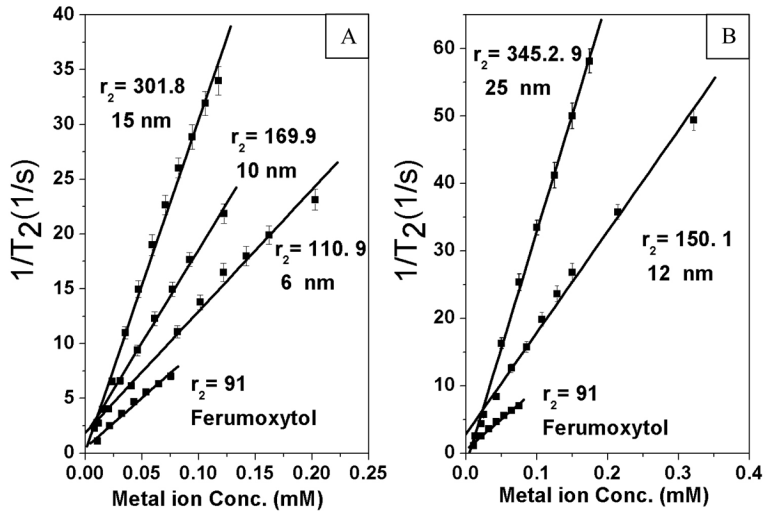

Figure 3.

Plot of $1/T_2$ Vs Metal ion concentration for A) spherical cobalt ferrite and B) FI cobalt ferrite nanostructures. Relaxivity coefficients r_2 were determined from the slop.

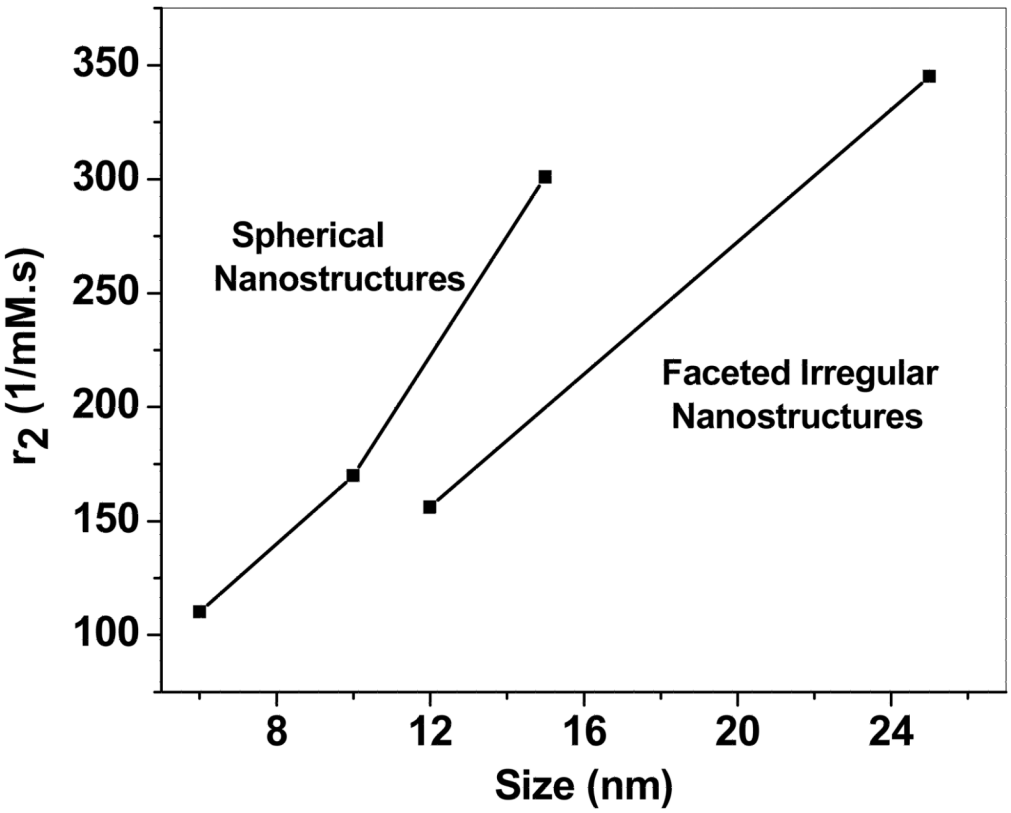

Figure 4.
Plot of relaxivity coefficient Vs magnetic nanostructure size. The solid lines were added to assist in visualization and distinction between different types of nanostructures

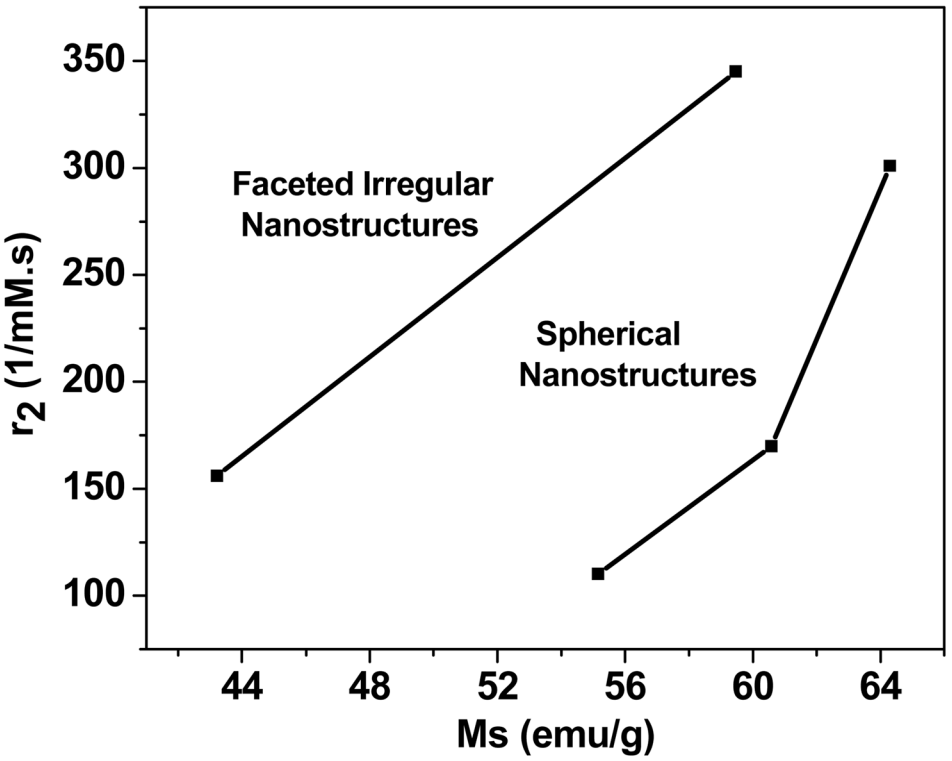

Figure 5.
Plot of magnetic saturation r_2 vs Ms i.e. relaxivity coefficient. The solid lines were added to assist in visualization and distinction between different types of nanostructure.

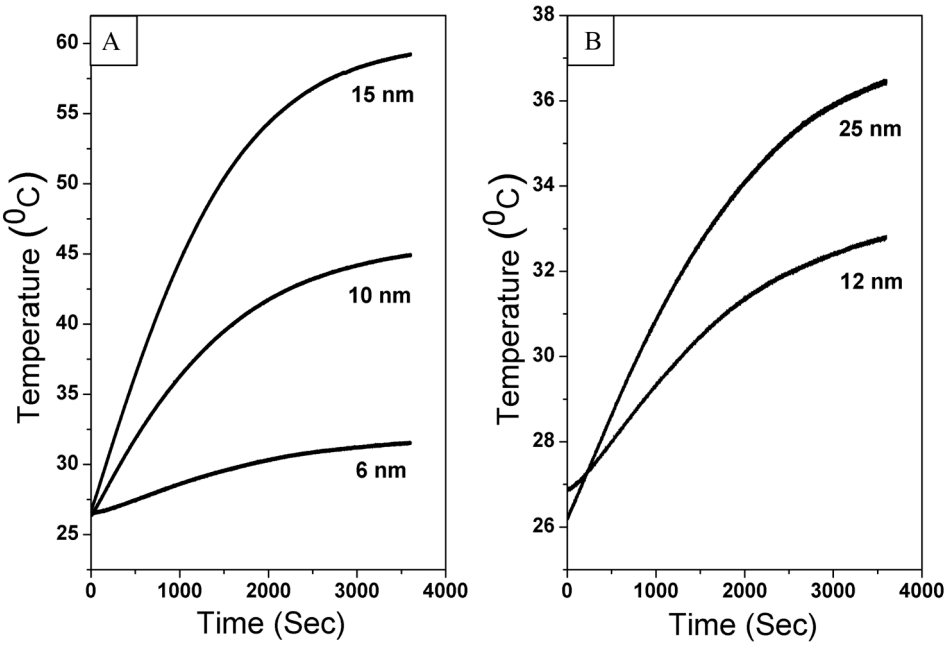

Figure 6.
Plot of Temperature Vs Time representing the thermal activation cobalt ferrite nanostructures in aqueous medium A) Spherical nanostructures B) FI nanostructures

Table 1

Saturation magnetization of various cobalt ferrite nanostructures

Shape	Size (nm)	M_s (e.m.u./g)
spherical	6 ±1.0	55.16
spherical	10±1.5	60.59
spherical	15±2.0	64.29
FI	12±2.0	43.22
FI	25±2.0	59.47

Table 2

Shape and size dependent RF thermal activation parameters

Geometry	Size (nm)	Magnetic saturation Ms (emu/g)	SAR W/g
Spherical	6	55.1	35.6
	10	60.5	231.4
	15	64.2	396.1
FI	12	43.2	55.5
	25	59.4	87.7